Heliyon 8 (2022) e11593

Contents lists available at ScienceDirect

Heliyon

journal homepage: www.cell.com/heliyon

Research article

Effects of cashew nutshell ash on the thermal and sustainability properties of cement concrete

Solomon Oyebisi [a,*], Festus Olutoge [b], Increase Oyaotuderekumor [a], Faithfulness Bankole [a], Hilary Owamah [c], Ugoh Mazino [a]

[a] Department of Civil Engineering, Covenant University, Ota, Nigeria
[b] Department of Civil and Environmental Engineering, University of West Indies, Trinidad and Tobago
[c] Department of Civil and Environmental Engineering, Delta State University, Abraka, Nigeria

HIGHLIGHTS

- CNA-PLC based concrete offers better thermal insulation characteristics.
- Environmental impacts of CNA-PLC based concrete decrease with increasing CNA content.
- Sustainability efficiency of CNA-PLC based concrete increases with increasing CNA content.

ARTICLE INFO

Keywords:
Cashew nutshell ash
Cement
Concrete
Environmental impacts
Recycling
Sustainability

ABSTRACT

The present study valorizes cashew nutshell ash (CNA) and uses it at 5–20 wt. % of cement for concrete production. The concrete grades of 25–40 MPa were used as mix design proportions. The thermal and mechanical properties of the concrete samples were determined on day 28 of curing. Regression models were used to predict the thermophysical properties of the concrete specimens. Also, the concrete's sustainability was estimated via the inventory of carbon and energy (ICE). The results revealed that CNA enhanced the thermal insulating characteristics of the concrete produced. Maximum compressive strength was obtained at 15 wt. % of CNA content, while the developed models yielded high precision. Compared with the control concrete, the sustainability index decreased as CNA content in the mix increased, indicating that incorporating CNA in concrete production improves the sustainability of such concrete. Therefore, the outcome of this work can be beneficial, especially in hot or arid climate regions, and at the same time, achieve a cleaner environment.

1. Introduction

The growing environmental challenges and energy usage are causing problems in the construction industry. The demand for energy and the environmental cost of producing it are both increasing [1, 2]. Buildings utilize over 40% of total global energy production; about 60 % is used for heating and cooling [3, 4]. In 2019, about 10 giga tonnes of carbon dioxide (CO_2) was reported as direct and indirect emissions from electricity and commercial heat due to the energy demand for heating and cooling with increasing harsh weather conditions and air-conditioning ownership [5]. Moreover, energy consumption increases with time [6]. Rapid industrialization and urbanization contribute to rising environmental issues and energy consumption [7]. Many civil engineering structures undergo temperature changes. Elongation occurs with increasing actual temperature; in contrast, contraction arises with decreasing actual temperature, thus leading to structural failure in bonding [8]. Therefore, building materials' thermal and physical properties are required to assess the thermal profiles of concrete members [8].

Natural resource conservation and environment protection are integral to national energy preservation in developing countries [9]. Therefore, adequate comfort buildings are based on proper insulation [9]. Apart from achieving good comfort for the building occupants, suitable insulation material can reduce the cooling pressure, generating considerable energy and cost savings [4] and reducing the discharge of carbon dioxide into the atmosphere from the power plants [10, 11, 12]. Liu et al. [13] stated that the building heat loss reduces with increasing thermal

* Corresponding author.
E-mail address: solomon.oyebisi@covenantuniversity.edu.ng (S. Oyebisi).

https://doi.org/10.1016/j.heliyon.2022.e11593
Received 14 September 2022; Received in revised form 18 October 2022; Accepted 8 November 2022

insulation characteristics, thus enabling energy-efficient buildings and improving environmental sustainability. Saygili and Baykal [14] noted that constructing buildings with better thermal insulation properties is more advantageous than making buildings with conventional construction materials due to the long-term advantages of reducing heating and cooling loss and decreasing the environmental pollution.

Concrete's thermal stability is influenced by the cement paste quality, presence of moisture, volume and distribution of pores, and the type of aggregate used [8, 15]. The thermal conductivity (TC), thermal diffusivity (TD), and specific heat capacity (SHC) of a building material play an essential role in the evaluation of its thermal performance based on the context of temperature exposure [16]. Furthermore, energy-efficient buildings depend on the thermal performance of the construction material, which signifies the flow of heat capacity through the material in the presence of temperature differences [17]. Therefore, low thermal conductivity requires construction material to reduce the absorbed heat into the building, particularly in the hot climate region [17].

Cashew nutshell is an agricultural waste product. The global generation of cashew nutshells in 2017 was about 4,430,341 metric tonnes. Out of this figure, Nigeria generated about 100,000 tonnes [18]. Furthermore, approximately 1,350,000 and 1,300,000 tonnes of cashew nuts were produced in West Africa and Asian regions [18, 19, 20]. Interestingly, cashew nutshell liquid, containing about 30–35 wt. % of cashew nutshell [21] can be used for automated chemical synthesisers [21], pharmaceutical drugs [22], and lubricants [23]. Godjo et al. [24] reported about 1,825,000 tonnes of waste from every 2,500,000 tonnes of cashew nuts. But these cashew nutshells are usually discarded indiscriminately, resulting in environmental problems.

Researchers have conducted studies, particularly in the construction department, to reduce energy consumption and environmental issues through the use of supplementary cementitious materials (SCMs); this contributes to energy and environmental protection and sustainable development [2, 25, 26]. For example, replacing cement with 10 wt% corn cob and wood waste ash, 20 wt% bagasse ash, and 30 wt% palm oil fuel rich shell ash improves the compressive strength of such mixed concrete [25]. Pavithra et al. [27] studied the behavior of concrete synthesized from chicken fibers with partial cement replacement by cashew nut shell ash (CNA). Replacing 8% cement with CNA containing 1% chicken feather fiber resulted in higher compressive, splitting and flexural strengths than the control concrete (cement concrete). Tantri al. [28] used CNA as a cementitious material to develop reclaimed asphalt pavements containing self-compacting concrete. The results showed that CNA is a cementitious material. Also 15% by weight CNA substitute is optimal as a substitute for OPC. The effects of SCM, class C fly ash, blast furnace slag, silica fume and rice husk ash have been studied on the thermal properties of concrete [15, 29]. The results showed that the incorporation of SCMs into the concrete mix reduces the thermal conductivity of such concrete. For example, without affecting the compressive strength, the replacement of cement by 15 wt% silica fume, 15 and 30 wt% fly ash, and 15 and 30 wt% slag reduced the thermal conductivity of the concrete by about 14, 12 and 23 and 11 and 18%, respectively. There have been few or no research on CNA despite the improved thermal insulation findings of different SCMs; this work fills that gap.

In the built environment, research has recently been focused on condensing the environmental impacts of building materials. The overall energy spent from direct and indirect material processes within the cradle-to-gate process is measured by embodied energy [30]. As stated by Hammond and Jones [30], Cradle-to-gate refers to the entire stream of materials from the ground up to the final processing operation's industry gate. Embodied carbon dioxide also adds to the fuel-associated carbon emissions that are deprived of accounting for the energy taken in the feedstock. Worldwide energy-associated CO_2 discharges were around 33 giga tonnes in 2019 [31], with the cement industry accounting for nearly 4.1 giga tonnes [31]. Construction consumes around $1/3^{rd}$ of global energy demand and discharges almost 40 % of direct and indirect CO_2 [5]. In 2021, worldwide energy-related CO_2 emissions are expected to rise by 4.8 % [32]. However, because of increasing demand, lowering worldwide energy-related CO_2 emissions while manufacturing cement to meet demand is difficult. The yearly cement production is predicted to rise considerably until 2030, while demand remains unchanged [32]. Captivating the benefit of agro-industrial symbiosis opportunities, for instance, using other byproducts to create a new product, a 0.8 % yearly drop is required to meet the 2030 sustainable development target [33]. These would assist in lowering the energy and emissions associated with carbon collection and utilisation [34, 35, 36].

Supplementary Cementitious Materials have been utilized as a partial or total replacement of Portland cement (PC) to reduce the environmental impacts of concretes [34, 37]. According to González and Navarro [38], using low-impact building materials can reduce carbon dioxide emissions by roughly 30 %. Furthermore, low-energy materials in the construction sector cannot be overemphasised: it helps reduce environmental degradation and production cost [39]. As a result, replacing Portland cement with SCMs cuts embodied energy and embodied carbon dioxide emissions considerably [36, 39]. Patil et al. [36] replaced ordinary Portland cement (OPC) with Volcanic Ash (VA) and investigated the impact of embodied energy on materials and buildings. When 50 wt.% of OPC was replaced with VA, the results demonstrated a 16 % reduction in embodied energy. In addition, replacing cement with about 25 wt. % of SCMs (rice husk ash, silica fume, and fly ash) result in 33 and 20 % decrease in energy demand and cost of materials [26]. Abubakar et al. [39] studied the environmental impacts of concrete modified with corn cob ash (CCA). The results showed that when the CCA level in the mixes increased, the embodied energy (EE) and embodied carbon dioxide emissions (EC) dropped. But in spite of several studies on the thermal and sustainability performance of blended cement concrete, little to no research has been done on concrete modified with CNA, which is why this study was conducted.

Differing from the existing literature, this study investigates the properties of concrete. Cashew nutshell ash was used as the SCM to assess the effects of CNA from thermal, mechanical, and sustainable standpoints and compare it with Portland limestone cement (PLC). PLC was replaced by 5–20 wt. % of CNA. The mixes were cured for 28 days, and the thermal properties and compressive strengths were determined. Model equations were developed to predict the thermal characteristics of the concrete produced using Matlab 2017a statistical software. Moreover, a simplified sustainability evaluation of CNA-cement-based concrete was carried out using the Inventory of Carbon and Energy (ICE). The results would enhance future studies by predicting the thermo-physical characteristics and depicting the concrete's sustainability.

2. Materials and methods

2.1. Materials

Cashew nutshell was sourced and valorised, obtaining about 25 wt. % of CNA. Table 1 presents the oxide elements of CNA and PLC used. The results revealed that CNA satisfied 70 % of the BS EN 450-1 [40] and BS EN 8615-2 [41] minimum criteria for silica, aluminate, and ferrite. The least quantum of 25 % SiO_2 [41] and the contents of MgO and SO_3 are 3 and 4 %, respectively [40], were met. Furthermore, ASTM C 618 [42] specified a 5% maximum loss of ignition (LOI) for any pozzolan, while BS EN 450-1 [40] and BS EN 8615-2 [41] recommended a 10% maximum for any pozzolan. Finally, the PLC's oxide elements complied with BS EN 196-3 [43].

The physical properties of the materials used are listed in Table 2. The specific gravity and surface area were calculated using BS EN 196-3 [43] experimental procedures, whereas fineness was assessed using BS EN 196-6 [44]. The particle size distribution of PLC and CNA was examined by laser diffraction (BC LS-100) and the results are depicted in Figure 1. CNA's specific gravity and mean particle size are lesser than PLC's, as indicated in Table 2. However, when CNA was substituted for PLC, fineness and specific surface area were higher, indicating that additional

Table 1. Chemical compositions of materials used.

Binding materials	Chemical compositions (%)										
	CaO	SiO_2	Al_2O_3	Fe_2O_3	MgO	K_2O	Na_2O	SO_3	TiO_2	P_2O_5	LOI
CNA	22.52	56.02	10.28	4.42	1.53	0.51	0.42	1.32	0.01	0.01	2.95
PLC	64.50	21.55	5.50	3.08	1.52	0.61	-	2.03	-	-	1.20

Table 2. Physical properties of materials used.

Properties	CNA	PLC	Fine Aggregate (FA)	Coarse Aggregate (CA)
Specific gravity	2.95	3.15	2.60	2.65
Fineness (%)	8.10	7.64	-	-
Specific surface area (m^2/kg)	525	375	-	-
Mean particle size (μm)	18.54	23.72	-	-
Water absorption (%)	-	-	0.70	0.80
Moisture content (%)	-	-	0.32	0.22

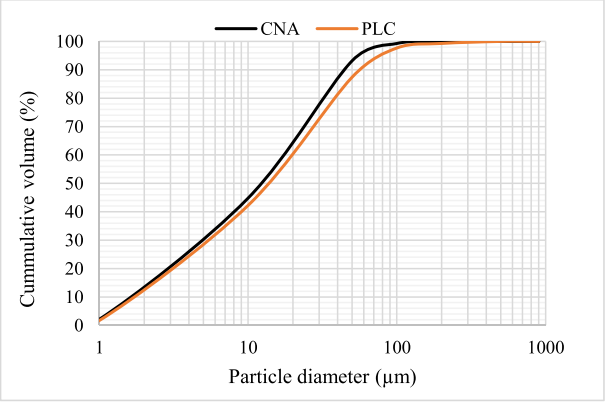

Figure 1. The particle size distribution of binding materials used.

volume and water were added [45]. These findings would aid CNA's ability to handle higher resistance in alkaline circumstances. Furthermore, the reaction of CNA with Portlandite from PLC would increase the concrete's capacity [45]. Similarly, the properties of the aggregates were investigated as per BS EN 12620 [46], as shown in Table 2. The fine aggregates were sharp sand with ≤4.5 mm sizes, while coarse aggregates were 12.5–19 mm granites. Furthermore, the grade was assessed using the BS EN 12620 [46] methodology, with the findings presented in Figure 2.

2.2. Sample design quantities

The sample mix proportioning was estimated based on BS EN 206 [47]'s method. Previous studies recommended a 20 % maximum substitution of CNA with PLC for structural purposes [48, 49, 50]. This was used to justify the CNA proportion. The proportioning of the design mixes for different grades (M25, M30 & M40) are detailed in Table 3 due to their wide applications in the built environment.

2.3. Experimental tests and analysis

2.3.1. Workability test

The mixing was carried out as per BS specifications [51]. The slump test was performed on the fresh mixes following the method detailed in BS EN 12350-2 [52].

2.3.2. Density test

The density test was conducted on day 28 following the BS EN 12390-7 [53] requirements. The mass of the specimens (m, kg) was weighed in a digital weighing balance, and the volume (v, m^3) was calculated. Therefore, the air-dry density (ρ, kg/m^3) was obtained using Eq. (1).

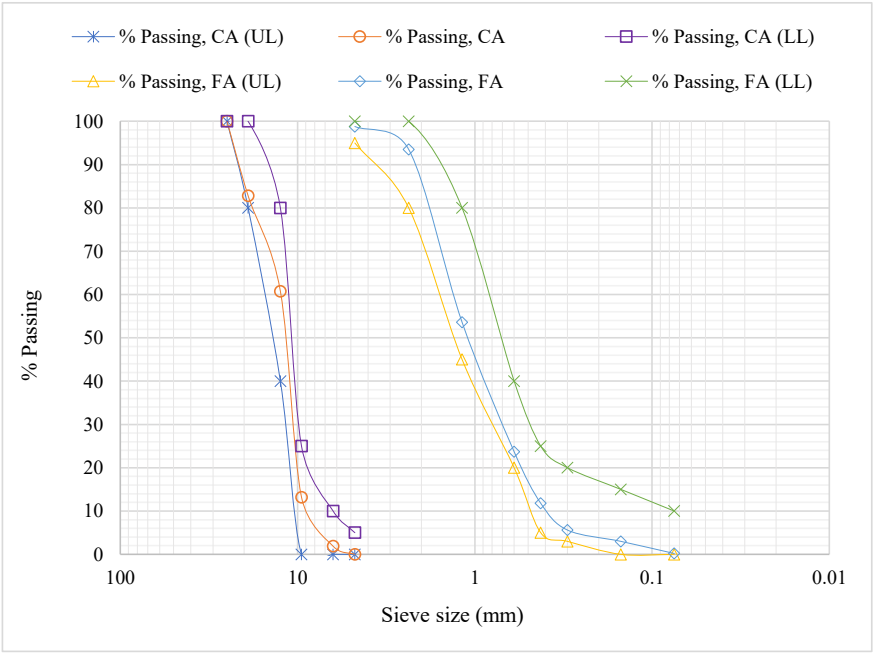

Figure 2. The PSD of aggregates used.

Table 3. Mix design quantities.

Concrete grade	Replacement level	Mix ID	PLC (kg/m^3)	CNA (kg/m^3)	FA (kg/m^3)	CA (kg/m^3)	W/B	A/B
M 25	100% PLC	R0	340	0	715	1035	0.62	5.15
	5% CNA	R1	323	17				
	10% CNA	R2	306	34				
	15% CNA	R3	289	51				
	20% CNA	R4	272	68				
M 30	100% PLC	R0	390	0	675	1031	0.54	4.37
	5% CNA	R1	370	20				
	10% CNA	R2	350	40				
	15% CNA	R3	330	60				
	20% CNA	R4	310	80				
M 40	100% PLC	R0	500	0	585	1031	0.42	3.23
	5% CNA	R1	475	25				
	10% CNA	R2	450	50				
	15% CNA	R3	425	75				
	20% CNA	R4	400	100				

W/B = water-to-binders (PLC + CNA) ratio; A/B = aggregates (FA + CA)-to-binders' ratio.

$$\rho = \frac{m}{v} \tag{1}$$

2.3.3. Compressive strength

The compressive strength (fc) was determined following the BS EN 12390-3 [54] procedure. The fresh concrete was mixed at 23 ± 5 °C and 65 % relative humidity, and filled the cube (150 × 150 × 150 mm^3) in three layers; each layer was tamped 25 times using a 16 mm diameter tamping rod to remove trapped air and ensure adequate compaction. The concrete cubes were kept in the mould for 24 h, demoulded, and immersed in a curing tank. After curing for 28 days, weights were recorded, and the cubes were transferred to the compression machine (Motorised COMTEST 2000 kN) for load applications at 3 kN/s of pace. The samples were double-checked and appropriately placed on the machine's base plate. The load was applied and maintained until the specimen failed. The load (kN) at failure was recorded. Thus, the compressive strength was computed using the applied load at failure (N) over the cube area (mm^2). For the test parameters, an average of three specimens were crushed.

2.3.4. Thermal conductivity (TC) test

The TC test was carried out on the concrete samples as per BS EN 12664 [55] procedure on day 28 using TD 1002 Heat Conduction Base Unit. The specimens were prepared using 30 mm diameter × 20 mm height cylinders. The samples' moisture content was removed by oven-drying at 105 °C for 24 h. Afterwards, the heat flow was set at 9.9 W for 10 min, and the temperature readings, as shown in Figure 3, were taken. Fourier's law governed the TC, which depends on understanding temperature distribution within the medium of heat flux [17]. However, Fourier's law is relevant in complex geometrics to transient and multi-dimensional conditions. Thus, the TC of the concrete samples was attained with the help of Fourier's law, as illustrated in Eq. (2).

$$k = \frac{\Phi \times t}{A \times \Delta T} \tag{2}$$

where, k = TC (W/mK); Φ = heat flow (W); t = thickness of specimen (m); A = area of the specimen (m^2); ΔT = temperature difference (K).

2.3.5. Specific heat capacity (SHC) test

The specimens were prepared using 50 × 50 × 50 mm^3 cubes. The SHC was determined following the electro-calorimetry method [7]. Before curing, two holes for both immersion heater (2000 W and 220–250 V capacity) and thermometer were made at 2/3 depth on the concrete samples using a 9 mm drilling bit. As displayed in Figure 4, the immersion heater and thermometer were inserted, and the samples were placed inside the calorimeter on day 28 of curing. Electricity was supplied at a particular period while temperature, current, and voltage were recorded continuously. It was reported that there is an increase in thermal expansion and temperature owing to the heat flow into the sample; however, the expansion and fluids are negligible and can be ignored [56, 57]. Therefore, the SHC, the amount of energy required to affect the temperature of 1 kg of the sample by 1 °C, was obtained using the relationship, as illustrated in Eq. (3).

$$c_p = \frac{Q_2 - Q_1}{(m_2 - m_1)(t_2 - t_1)} \tag{3}$$

where c_p = SHC at a constant pressure (J/kgK); Q_1 and Q_2 = initial and final heat energy (J); m_1 and m_2 = initial and final mass of the sample (kg); t_1 and t_2 = initial and final temperature (K).

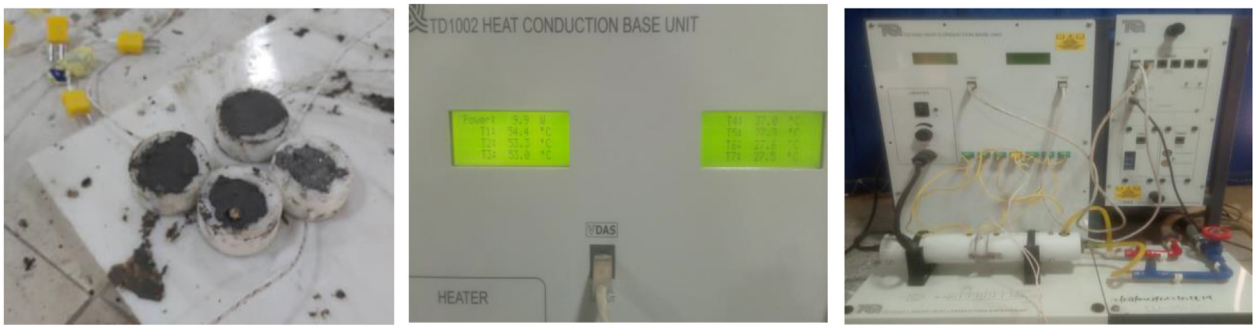

(a) (b) (c)

Figure 3. (a) Specimens (b) Thermal readings (c) TD 1002 Heat Conduction Base Unit.

Figure 4. Specific heat capacity set up.

2.3.6. Thermal diffusivity (TD) test

Thermal diffusivity shows how a sample responds to temperature changes [8]. Hence, the TD was calculated using the relationship, as illustrated in Eq. (4) [8, 58].

$$\alpha = \frac{k}{\rho c_p} \tag{4}$$

where α = TD (mm^2/s); k = TC (W/mK); ρ = density of the sample (kg); c_p = SHC at a constant temperature (J/kgK).

2.3.7. Model equations for the prediction of concrete thermal properties

The best physical property of concrete that relates to the thermal properties, TC and TD of concrete is density [59]. Consequently, this study predicted the relationship between the density and the earlier mentioned thermal properties. Besides, the models between TC and SHC, TD and SHC, and TD and porosity were presented to correlate both TC and TD to the material's thermal storage capacity in the surrounding temperatures and porous material, especially when concrete is mixed with pozzolanic materials. Furthermore, the SHC of concrete is affected mainly by the aggregate types and distribution and surrounding temperature. Thus, compared with TC and TD, SHC shows no strong correlation with the density [8, 59]. The projected model equations were developed with the help of a regression model using the Matlab R2017a statistical software tool. Moreover, the developed equations from this study were validated using experimental results obtained from earlier works to judge and validate the accuracy of the empirical equations, which depend highly on the experimental results. As demonstrated in Eq. (5), the model exponential was implemented for the prediction because an exponential relationship occurs between the TC and concrete density [58, 59, 60].

$$k = ae^{bp} \tag{5}$$

where k = TC (W/mK); a and b = coefficients (at 95% confidence bounds); p = air-dry density of the concrete sample (kg/m^3).

2.4. Sustainability assessment

2.4.1. Environmental impacts

The inventory analysis was used to estimate the embodied energy and carbon dioxide emissions of the materials used to produce the concrete within the cradle-to-site confinement. This boundary includes both cradle-to-gate and transportation to the final destination [30]. On applying to real-world case studies, the inventory model equations, as shown in Eqs. (6), (7), (8), (9), (10), and (11), have superior accuracy and flexibility to other methods [30]. By applying the coefficient of energy and emission factors, the inventory technique eliminates the complicated procedures that require chemical equations.

$$Cradle - to - site\ EE = Cradle - to - gate\ EE + Transport\ EE \tag{6}$$

$$Cradle - to - gate\ EE = \sum_{i=1}^{n}(M_i \times EE_i) \tag{7}$$

$$Cradle - to - site\ EE = (1+m)\left(PLC_{xplc} + CNA_{xcna} + CA_{xca} + FA_{xfa} + W_{xw}\right) + TEE \tag{8}$$

$$Cradle - to - site\ EC = Cradle - to - gate\ EC + Transport\ EC \tag{9}$$

$$Cradle - to - gate\ EC = \sum_{i=1}^{n}(M_i \times EC_i) \tag{10}$$

$$Cradle - to - site EC = (1+n)\left(PLC_{xplc} + CNA_{xcna} + CA_{xca} + FA_{xfa} + W_{xw}\right) + TEC \tag{11}$$

where M_i = material's weight (kg),
EC = embodied carbon dioxide emission of concrete produced ($kgCO_2/m^3$),
EE = embodied energy of concrete produced (MJ/m^3),
EE_i = embodied energy coefficients (MJ/kg),
EC_i = embodied carbon dioxide emission factors ($kgCO_2/kg$),
PLC, CNA, CA, FA, and W = weights (kg) of Portland limestone cement, cashew nutshell ash, coarse aggregates, fine aggregates, and water, respectively,
xplc, xcna, xca, xfa, and xw = embodied energy coefficients (MJ/kg) and embodied carbon dioxide emission factors ($kgCO_2/kg$) of the materials listed above,
n and m = wastage factors (%) of EE and EC, taking as 22 and 19 %, respectively [61],
TEE and TEC = transport embodied energy (MJ/m^3) and transport CO_2 emissions ($kgCO_2/m^3$) of the final product, respectively.

Waste materials are assumed to have zero embodied energy and carbon dioxide emissions [39, 62]. As a result, cashew nutshell contains zero EE and EC at the collection point. On the other hand, CNA is dehydroxylated at a regulated temperature of around 400 °C for 2 h. Consequently, the valorization of cashew nutshell to produce CNA results in energy consumption and CO_2 emission. Hence, the EE and EC of the CNA were estimated via the EE of liquefied petroleum gas (LPG) used to power the furnace pyrolyzer as follows:

A 12 kg of LPG was used to power the furnace. The initial EE of LPG is taken as 3.45 MJ/kg [39].

$$Total\ EE\ of\ burning\ 12\ kg\ of\ LPG = 12 \times 3.45 = 41.40\ MJ$$

Approximately 30 kg of CNA was obtained using 12 kg of LPG for the valorization process. Thus, EE of CNA = 41.40/30 = 1.38 MJ/kg. Hammond and Jones [63] established a correlation between the environmental impacts, as exemplified in Eqs. (12), (13), and (14), respectively.

$$EC_e\ (kg) = 0.021 \times EE \tag{12}$$

Table 4. EE coefficients and EC factors for concrete ingredients.

Constituent	EE_i (MJ/kg)	EC_i ($kgCO_2/kg$)	Source
PLC	55×10^{-1}	95×10^{-2}	[30]
CNA	13.8×10^{-1}	8×10^{-3}	This study
FA	8.1×10^{-2}	4.8×10^{-3}	[30]
CA	3×10^{-1}	1.7×10^{-2}	[30]
Water	1×10^{-2}	1×10^{-3}	[30]

$$EC_e = 3.67 \times CO_2\ (kg) \tag{13}$$

$$EC\ (kg) = 0.0057 \times EE \tag{14}$$

Applying Eq. 14: $EC\ (kg) = 0.0057 \times 41.40 = 0.236\ kg\ of\ CO_2$

Therefore, $CO_2\ emission\ per\ kg\ of\ CNA\ (EC) = \frac{0.236}{30} = 0.008\ kgCO_2/kg$

Table 4 presents the EE coefficients (EE_i) and EC factors (EC_i) of materials used to produce CNA-cement-based concrete.

2.4.2. Transport EE and EC

Fuel energy is consumed, and carbon dioxide is emitted during the transportation of construction materials. As a result, the energy and carbon dioxide are embodied in the construction materials. Linear model, as illustrated in Eq. (15), was developed by Bribian et al. [64] to evaluate the embodied energy and embodied carbon dioxide emissions. Table 5 indicates the required coefficients to be applied by different ways of transportation to determine the material's transport impact of one tonne.

$$Transport\ impact = c_1 d_1 + c_2 d_2 + c_3 d_3 \tag{15}$$

where d_i = distance travelled by each type of transportation (km)
c_i = coefficients applied to each type of transportation.

Table 6 presents the production/collection source, average haulage distance, and contact coordinates of each construction material to the laboratory.

2.4.3. Sustainability index (S_i)

As illustrated in Eq. (16), the concrete's sustainability index (S_i) was quantified to assess the concrete's sustainability by comparing the environmental factors with strength performance [65].

$$S_i = \frac{EC + (CO_{2i} \times EE)}{f_c} \tag{16}$$

CO_{2i} is taking as 0.050 $kgCO_2/MJ$ [65], and f_c = concrete's compressive strength at 28-day (MPa).

3. Results and discussion

3.1. Slump

Figure 5 displays the slump results for M 25, M 30, and M 40. The results indicated that the slump was reduced upon increasing the CNA content in the mix. At 5–20 wt. % of CNA replacement, there was about 13–40 %, 10–43 %, and 8–47 % decrease in slump for concrete grades 25, 30, and 40, respectively. The reason could be associated with the physical characteristics of CNA, which exhibit lesser specific gravity and particle size than PLC. As a result, CNA's volume increases while water demand also increases as CNA replaces PLC, resulting in more cohesive concrete and reducing the concrete's workability [45]. These results corroborate the previous findings that incorporating CNA reduces the concrete slump [48, 49, 66]. Ultimately, a substantial modification with CNA could be a workable mix up to 20 % substitution because an optimum 150 mm of workable concrete recommended by BS EN 12350-2 [52] was met.

Table 5. EE and EC coefficients for transporting material of 1 tonne.

Impact Group	Truck, Road (c_1)	Freight, Rail (c_2)	Transoceanic, Ship (c_3)	Source
Primary energy demand (MJ-Eq/km)	3.266	0.751	0.170	[64]
Global warming potential ($kgCO_2$-Eq/km)	0.193	0.039	0.011	[64]

Table 6. Average haulage distances (AHD) of each construction material.

Material	Source of collection	AHD (km)	Coordinates
PLC	Ibese, Nigeria	62.0	7.00546, 3.04870
CNA	Owode-Yewa, Nigeria	17.0	6.71228, 2.97523
FA	Abeokuta, Nigeria	81.0	7.14761, 3.36195
CA	Abeokuta, Nigeria	81.0	7.14761, 3.36195
Water	Covenant University, Nigeria	0	6.68733, 3.15802

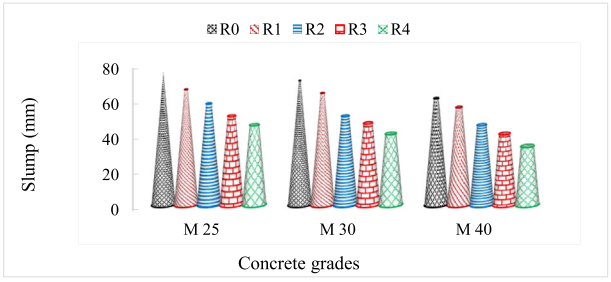

Figure 5. The slump results.

3.2. Density

Figure 6 shows the density findings on day 28 of curing. When the CNA concentration in the mixes was increased, the density dropped. CNA replacement increased from 5-20 wt.% for all levels of concrete grade strengths, resulting in a 3–11 percent drop in density when compared to the control concrete (R0, 100 % PLC). The specific gravity of CNA is 10 % lower than that of PLC (Table 2), which reduces the interfacial particle of PLC and lowers the density [67].

Also, Figure 6 indicates an increase in density upon increasing the concrete grades (M 25–40) due to the effects of the aggregate-cement ratio (Table 4). It may also be attributed to the concrete mix's denser, less porous, and low water content [45]. These findings corroborate previous results where concrete with a lower mix grade (1:3:6), having a higher aggregate-cement ratio, exhibited lower density than concrete with a higher mix grade (1:1.5:3) [67]. Aggregate content increases the

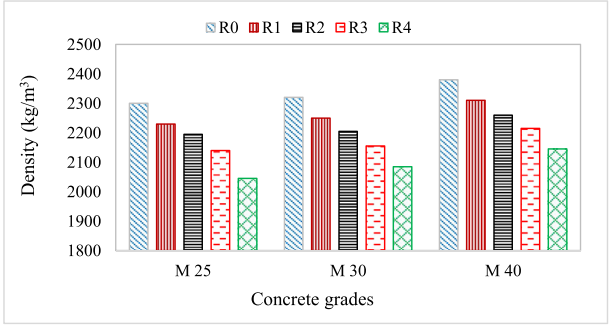

Figure 6. The density of concrete grades.

concrete's void content while decreasing the concrete compactness level. Thus, replacing PLC with CNA reduces the building's dead loads.

3.3. Compressive strength (fc)

Figure 7 shows the compressive strengths for M 25, M 30, and M 40 on day 28 of curing. It was observed that as CNA substitution increased, the strength also increased. As the percentage substitution of CNA content increased from 5-15 %, there was about a 3–6 % increase in strength for all samples at 28 days of curing compared with R0 (100 % PLC). The reasons may be associated with CNA's silica (SiO_2) and alumina (Al_2O_3) contents, as indicated in Table 1, being higher than PLC's. These elements, when reacting with the PLC's hydrating agents, result in the strengthening gel (C–S–H) and strengthening bond (C-A-H) of concrete, thereby increasing the strength [45]. However, at 20 wt. % of CNA substitution, a slight reduction in compressive strength was observed compared with other replacement levels for all concrete grades. This performance could be attributed to the slow reactivity of CNA's silica with PLC's Portlandite ($Ca(OH)_2$), delaying the C–S–H formation and retarding the strength development [48]. Notwithstanding, there was a strength satisfaction, even at 20 wt. % of CNA substitution compared with the control concrete. These results align with previous findings where 20 % of CNA with 2 % of chicken feather fibre resulted in about 8 % increase in compressive strength compared with the control concrete on day 28 of curing [68]. The density functional mechanism, which reveals the strength of structures more unbiasedly, could also be responsible for this strength development [69, 70].

It was also noticed from Figure 7 that the compressive strength of CNA-cement-based concrete increased with increasing concrete grade due to the aggregate-cement ratio of the concrete mix. The increase in aggregate-cement ratio reduces the cement content that bonds the aggregates, reducing the compressive strength of CNA-cement concrete. However, a higher concrete grade mix possesses a lower aggregate-cement ratio and reduces the concrete voids, enhancing the compactness level [67]. Consequently, cement particles fill aggregate spaces, strengthening the aggregate's physical packing and hydrating processes, which improve the concrete's strength [8, 67].

Ultimately, CNA can be applied for structural purposes at 5–20 wt. % replacement level because all concrete grades satisfied the target strengths BS EN BE EN 1992-1-1 [71] recommended on day 28 of curing.

3.4. Thermal conductivity (TC)

As shown in Fig., the thermal conductivity decreased as CNA content in all mixes increased. Less air was entrapped with increasing CNA content within the combinations, reducing the heat transfer rate through the concrete. The decrease in TC with increasing CNA content in the concrete mix could be attributed to CNA's lesser specific gravity and density than PLC, contributing to the reduction in TC of the concrete mix [15, 72]. The density of concrete significantly contributes to the TC of material because TC reduces with decreasing concrete density [8, 15]. This is evident from the earlier findings, where a 3 % decrease in concrete density reduced TC by 11 % on day 28 [73]. As illustrated in Figure 6, the concrete density decreased with increasing CNA content in the mix, contributing to the decrease in TC of the concrete.

It was also evident from Figure 8 that the TC of M 25 was marginally lower than M 30 and M 40 at the exact replacement of CNA content in the mixture. The mix of concrete grade 40 (M 40) was denser than M 25 and M 30 mixes due to low water-to-cement, resulting in a more durable cementitious matrix. Moreover, TC increases with increasing cement content [8]. Although, during the heat transfer, moisture content becomes the dominant factor. The thermal conductivity increases with increasing the water-to-binder ratio because the TC of water is around 50% lesser than that of hydrated cement paste [8]. However, the number of macropores in the concrete matrix increases with increasing the water-to-binder ratio, reducing the density and decreasing the TC.

The results also revealed that the concrete aggregate-to-cement ratio influences the TC of CNA-cement concrete. As shown in Figure 8, concrete grade M 25 mix with a higher aggregate-cement percentage exhibited a 1.28 W/mK for control (R0) compared with 1.31 W/mK of TC for concrete grade M 40 mix with a lower aggregate-cement ratio of the same mix sample. Thus, it can be deduced that the TC of concrete mix increases with increasing concrete grade. This deduction is in line with Raheem et al. [67]. They reported that the TC of concrete incorporated with RHA and PKSA for concrete grade M 20 mix, with a higher aggregate-cement ratio, was 0.60 and 0.29 W/mK lower than concrete grades 25 and 30 mixes. Also, similar findings were reported by Howlader et al. [74], where a higher aggregate-cement ratio concrete mix (1:2:3) yielded lower TC than a lower aggregate-cement ratio concrete mix (1:1.5:2).

Conversely, the TC reduces with increasing CNA content in the concrete mix at all grade levels. However, only 20 wt. % CNA substitutions with PLC at all grade levels (R4) satisfied a TC of 1.0 W/mK maximum for lightweight aggregate concrete, as recommended by Newman [75], Newman and Owens [76], and RILEM [77], hence beneficial for insulation application. Therefore, without compromising the strength performance, incorporating 20 wt. % of CNA as a partial replacement for PLC in concrete production in the building environment would reduce the heat transfer rate, thereby increasing the thermal insulation properties of the concrete, attaining acceptable comfort buildings, and enhancing environmental sustainability.

3.5. Specific heat capacity (SHC)

Figure 9 reveals an increase in SHC as the content of CNA in the mix increased for all levels of concrete grades. The results could be attributed to lower density of CNA, which increases the energy required to raise the material's mass by the unit temperature at constant pressure. Consequently, the potential heat of concrete rises, increasing the SHC [15, 78].

It was also observed that the SHC increased upon decreasing the concrete density. This Agrees with the results reported in related studies [8, 67, 73, 79]. The SHC of concrete increased with decreasing density, requiring higher heat to raise its unit weight by a unit temperature.

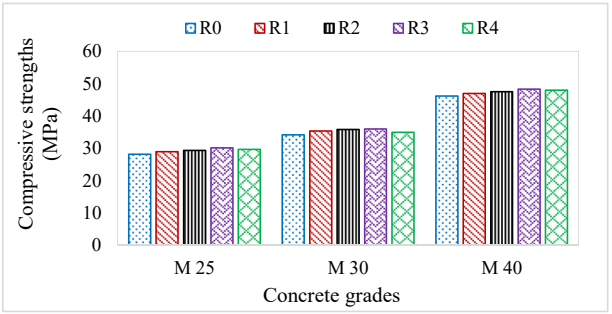

Figure 7. Compressive strengths for concrete grades.

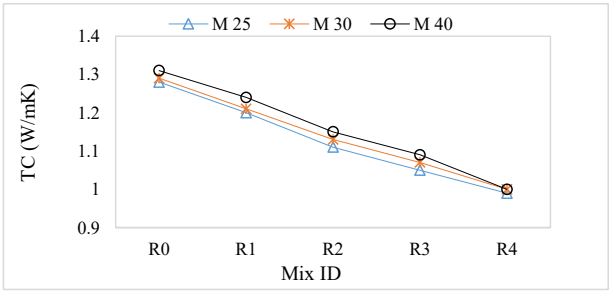

Figure 8. TC of concrete produced at 28 days curing.

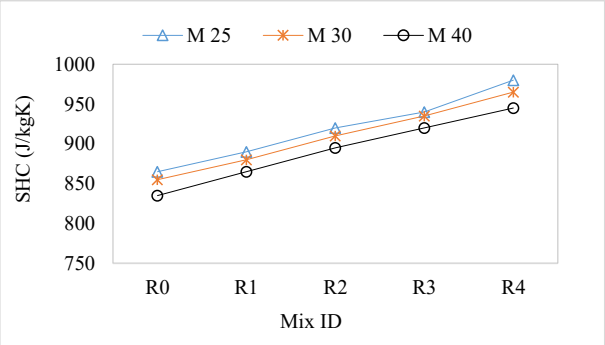

Figure 9. SHC of concrete produced at 28 days curing.

From Figure 9, it was revealed that M 25 exhibited higher SHC than M 30 and M 40. The reason could be associated with the higher water-to-binder ratio of M 25 mix because the SHC of water is much larger than that of any other concrete constituent, being 4190 J/kg K at 23 °C [8]. Furthermore, the aggregate-to-cement ratio influences the SHC of concrete [67, 74]. As a result, an increase in SHC of M 25 in this study could be ascribed to the fact that M 25 has the highest aggregate-to-cement ratio compared with M 30 and M 40. These assertions are consistent with Raheem et al. [67] 's findings, who reported that the SHC of M 20 with the highest aggregate-to-cement ratio was 600 and 940 J/kgK, higher than M 25 and M 30, respectively. Howlader et al. [74] also found that concrete mix proportion (1:2:3) with a higher aggregate-to-cement ratio yielded higher SHC than concrete mix (1:1.5:2) with a lower aggregate-to-cement ratio. Ngohpok et al. [80] posited that concrete mix with a high aggregate-to-cement percentage exhibits an increase in filling paste and void content compared with a low aggregate-to-cement ratio, hence an increase in SHC.

Ultimately, the results obtained are within the relevant values ranging from 840-1170 J/kgK for average weight aggregate [8] and 837–1074 J/kgK (1400–1900 kg/m^3 of density) for lightweight aggregate concrete [81]. Therefore, this study has shown that incorporating CNA into concrete production results in higher thermal insulation characteristics than PCC because it takes longer to absorb heat from the environment, thereby minimising the temperature incidence within the building.

3.6. Thermal diffusivity (TD)

The results of the TD of the concrete are presented in Figure 10. Notably, the results followed a similar pattern as shown for TC in all levels of concrete grades. It was observed that the TD was reduced upon increasing the CNA content in the concrete mix. It has been reported that TD is directly related to the TC and concrete's density, such that what affects TC also affects the TD of concrete [82]. Thus, the decrease in TD of CNA-cement-based concrete could be ascribed to the enclosed pores in CNA, reducing the density and TC of concrete and decreasing the concrete TD [82].

Previous studies also reported that the SCM with a lesser specific gravity and higher SiO_2 content than cement reduced the thermal diffusivity of concrete [72, 73]. Consequently, the differential temperatures between indoors and outdoors would be longer than the usual period to equilibrium due to the lower TD of CNA-cement-based concrete than the conventional concrete. Thus, low TD concrete exhibits slow reactions to temperature differences, resulting in an efficient thermal mass composite in a building [58].

As shown in Figure 10, it was also noticed that the concrete's TD increased upon increasing the concrete grade levels; this can be attributed to a low aggregate-to-cement ratio with increasing concrete grade mix. For example, the TD of control concrete (R0) for M 25 with the highest aggregate-to-cement percentage was 0.01 and 0.04 mm^2/s lower than M 30 and M 40, respectively. The M 25 includes more aggregate proportions than M 30 and M 40, reducing cement content and increasing concrete voids, thereby decreasing the concrete density and TD. These results establish the similar findings reported by Raheem et al. [67]. The TD of the control concrete grade (M 20) with the highest aggregate-cement ratio was 0.15 and 0.02 mm^2/s lower than concrete grade mix M 25 and M 30, respectively. In a related finding, Howlader et al. [74] reported an increase in concrete's TD with a higher-grade mix (1:1.5:2) having a lower aggregate-cement ratio than a lower-grade mix (1:3:6) with a higher aggregate-cement ratio.

On day 28 of curing, the TD of CNA-cement-based concrete satisfied the TD range of 0.55–1.55 mm^2/s recommended by Neville [8]. Ultimately, the incorporation of CNA offers a low reaction rate to thermal temperature. These findings can also be applied in mass concreting or relevant building construction where hot climate condition is perturbing to act as a heat sink/source to absorb extreme temperatures experienced during a thermal cycle.

3.7. Development of model equations

3.7.1. Relationship between TC and density

On day 28 of curing, Figure 11 depicts the relationship between the TC and the density of CNA-cement-based concrete. The coefficient of determination (R^2) was 95 % suited to anticipate the link between the TC and the density of the concrete. Furthermore, the sum of squared errors (SSE), a network performance function, which measures the model's performance between 0 and 1, efficiently regularised the model because the SSE value was closer to zero [83]. Moreover, the root means square error (RMSE), which measures the spread of data points around the regression line, indicated that the regression line fits the data because the closer the RMSE value to zero, the better the data meets the regression line [84]. Thus, as illustrated in Eq. (17), the model equation of CNA-cement-based concrete exhibited a strong correlation and yielded

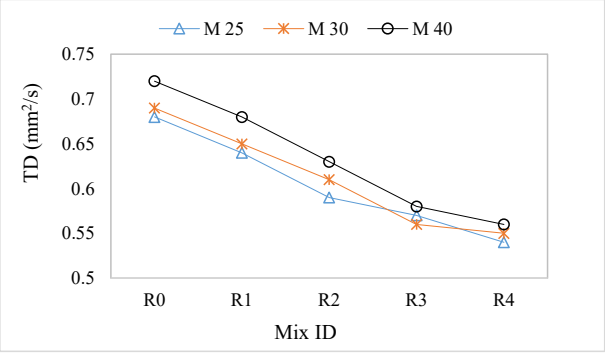

Figure 10. TD of concrete produced at 28 days of curing.

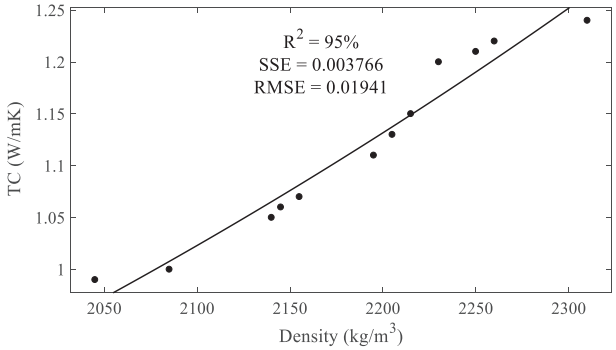

Figure 11. Relationship between TC and density.

high precision (R^2 = 95 %) at 95 % confidence bounds. This model equation (Eq. 17) agrees with the exponential correlation between TC and the density of RHA-blended PSKA concrete developed by Raheem et al. [67]. The coefficient correlation was 94 % R^2 for concrete grades ranging from M 20 to M 30. This model equation can predict the relationship between TC and the density of concrete incorporating CNA.

$$k = 0.1229e^{0.001009\rho} \quad (17)$$

where k = TC (W/mK) and ρ = density (kg/m^3).

3.7.2. Relationship between TC and SHC

Figure 12 shows the connection between TC and SHC of CNA-cement-based concrete on day 28 of curing. As shown in Figure 12, the R^2 value was 94 % acceptable to forecast the connection among the TC and SHC of the concrete, indicating the strong correlation and high precision at 95 % confidence bounds. A limited model predicts the relationship between the TC and SHC of concrete incorporating SCMs. However, as given in Eq. (18), the proposed model equation can be applied for predicting TC and SHC of concrete incorporating CNA and SCMs.

$$k = 8.18e^{-0.002164Cp} \quad (18)$$

where k = TC (W/mK) and c_p = SHC (J/kgK).

3.7.3. Relationship between TD and SHC

Figure 13 illustrates the correlation between TD and SHC of CNA-cement-based concrete on day 28 of curing. It was revealed that R^2 was 92 % fit to predict the relationship between the TD and SHC, yielding a high precision at 95 % confidence. After extensive review, the authors found no previous correlation between the TD and SHC of blended cement concrete to affirm the developed correlation (Equation 19). Therefore, as shown in Eq. (19), the developed model can predict the correlation between the properties examined for the concrete produced.

$$\alpha = 4.167\ e^{-0.002114Cp} \quad (19)$$

where α = TD (mm^2/s) and c_p = SHC (J/kgK).

3.7.4. Relationship between TD and density

Figure 14 illustrates the association between TD and CNA-cement-based concrete density on day 28 of curing. The coefficient of determination, R^2 of 87 %, indicated a high precision and strong correlation between the relationships at 95 % confidence bounds. The exponential correlation developed by this study, as illustrated in Eq. (20), agrees with the earlier developed correlation model, where the relationship between the TD and density of the RHA-blended PSKA concrete yielded a coefficient correlation (R^2) of 94 % [67]. Thus, the proposed model equation illustrated in Eq. (20) can be used to predict the relationship between the TD and the density of concrete incorporating CNA.

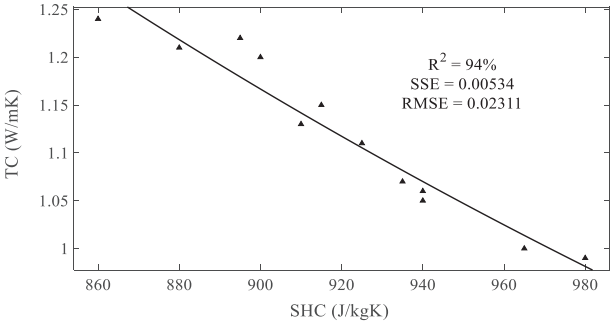

Figure 12. Relationship between TC and SHC.

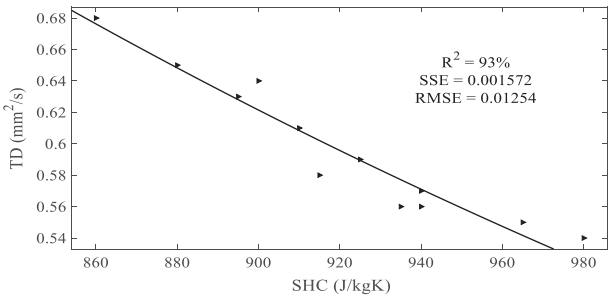

Figure 13. Relationship between TD and SHC.

$$\alpha = 0.07611\ e^{0.009408\rho} \quad (20)$$

where α = TD (mm^2/s) and ρ = density (kg/m^3).

3.8. Validation

3.8.1. TC and density

Following the model equation illustrated in Eq. (17), the validity of TC and density on day 28 of curing is presented in Figure 15. The Predictive Thermal Conductivity (PTC) and Experimental Thermal Conductivity (ETC) showed a similar pattern and trend with the predictive model, confirming a good agreement and relationship. Moreover, Demirboga [15] utilized various SCMs as a partial replacement, ranging from 7.5-30 wt. % of cement. It was evident from Figure 17 that there was a high precision with 85 % R^2, indicating a strong relationship. The model equation (Equation 17) also exhibited a strong correlation with the results reported by Karakoc and Demirboga [85] and Khan et al. [86] with 100 and 95 % R^2, respectively. Therefore, this developed model equation can predict the TC of concrete incorporating various SCMs at a targeted air-dry density ranging from 2000-2320 kg/m^3; this would save time and cost in experimental laboratory work.

3.8.2. TD and SHC

The validated results of TD with specific heat capacity are presented in Figure 16, following the proposed model equation illustrated in Eq. (19). The predictive thermal diffusivity (PTD) and experimental thermal diffusivity (ETD) yielded high precisions at 81 and 98 % R^2 for Gomel et al. [59] and Mydin [87] results, respectively, proving a good relationship. Therefore, this developed model equation (Equation 19) can be applied to predict the TD of concrete incorporating SCMs at a targeted SHC ranging from 840-980 J/kgK.

3.8.3. TD and density

Figure 17 presents the statistically validated results between TD and density following the established model equation shown in Eq. (20). The regression model yielded a high precision with 95 % R^2, confirming a good association at a 95 % confidence level. Hence, this developed model equation (Equation 20) can predict the TD of concrete modified with SCMs at a targeted air-dry density ranging from 2000-2320 kg/m^3.

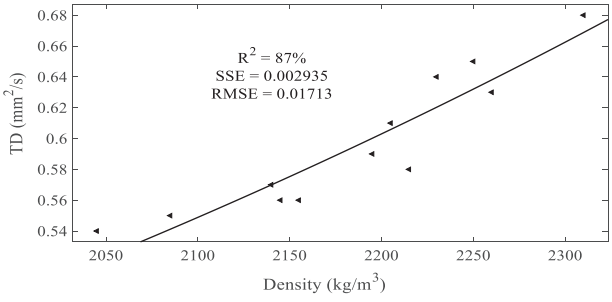

Figure 14. Relationship between TD and density.

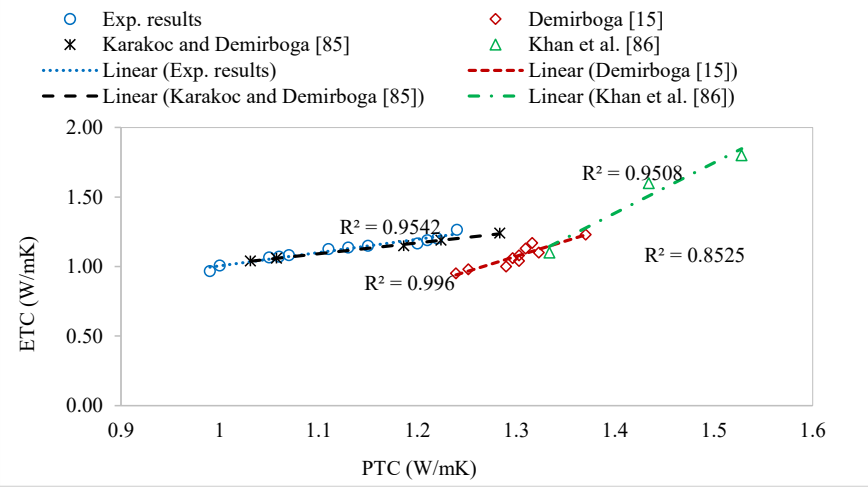

Figure 15. Validation of the developed model (Equation 17) with the previous studies.

3.9. SEM micromorphological analysis

Figure 18 presents the SEM micromorphology analysis conducted on the CNA-cement-based concrete to characterize the microstructures at 28 days of hydration using Phillips PW-1800. Each sample was crushed and pulverized for 1 min using Simatic C7-621. After that, pellets were made from the pulverized specimen by grinding 20 g of each sample with 0.4 g of stearic acid for 1 min. A 1 g of stearic acid was measured and placed in an aluminium cup and allowed to pass through a 2000 kN of pressure. The SEM voltage and analysis working distance were fixed at 5.0 kV and 46.72 mm. A 2 mm pellets were added into the XRF sample holder for analysis. The internal structure of the control sample (R0, 100 % PLC), as indicated in Figure 18(a), showed good densification, wrinkled shape, compactness, and low pores. The micromorphology was flaked with calcium-silicate-hydrate due to the reaction between calcium oxide (CaO) present in PLC and the water [48]. Compared with Figure 18(a), the SEM micrographs of Figure 18(b) revealed crystalline and reticular internal structures with good compactness and uniform matrix. The micromorphology exhibited calcium-silicate-hydrate gel due to the chemical reaction between Portlandite in PLC and aluminosilicate monomers in CNA [48]. The internal pores in the CNA-cement-based samples were reduced upon increasing CNA due to the CNA's filler effect [45].

3.10. Sustainability assessments

3.10.1. Embodied energy (EE)

Figure 19 indicates the transport embodied energy (TEE) of each material tonne in line with the details outlined in Tables 3, 5, and 6, and Eq. (15), using road as means of transporting each material from the production/collection source to the laboratory. The transport embodied energy, particularly for CNA, in Figure 19 is vanishingly small due to its low energy coefficient compared to other concrete components.

Figure 20 illustrates the concrete's EE based on the analyses outlined in Tables 3 and 4, Figure 19 and Eq. (8). The results indicated a decrease in embodied energy as CNA in the concrete mix increases. The reasons could be attributed to the CNA's initial EE (EEi), which is 75 % lower than PLC. Reducing the embodied energy of construction materials condenses the concrete's embodied energy [36, 62, 88, 89]. From Figure 20, the embodied energy decreased from 3265.23-2913.44 MJ/m^3, 3593–3179.93 MJ/m^3, and 4321.47–3804.14 MJ/m^3 for M 25, M30, and M 40, respectively, as CNA in the concrete mix increased from 0-20 wt. %. These reductions signified about 3–12 % embodied energy savings at 5–20 wt. % replacement of PLC with CNA for all concrete grade mixes. These results align with Abubakar et al. [39], where about 3–12 % of EE savings were attained at the partial substitution of OPC with 5–20 wt. % of corn cob ash (CCA). Moreover, Patil et al. [36] discovered a 16 % reduction in embodied energy once OPC was substituted with 50 wt. % of natural pozzolanic volcanic ash.

It was also observed from Figure 20 that the embodied energy increased upon increasing the concrete grade mix. The reasons could be ascribed to a high binder-to-aggregate ratio with increasing concrete grade mix [89]. Compared with M 25, there were about 17. 40 and 38.70 % rise in binder-to-aggregate ratios for M 30 and M 40, respectively. In addition, PLC contributes approximately 75.64 % of embodied energy to CNA-cement-based concrete production. The results at this juncture validate the energy reduction due to incorporating CNA into the concrete mix. Besides, the production process of CNA is less energy-intensive than PLC. Therefore, the embodied energy assessment infers that CNA

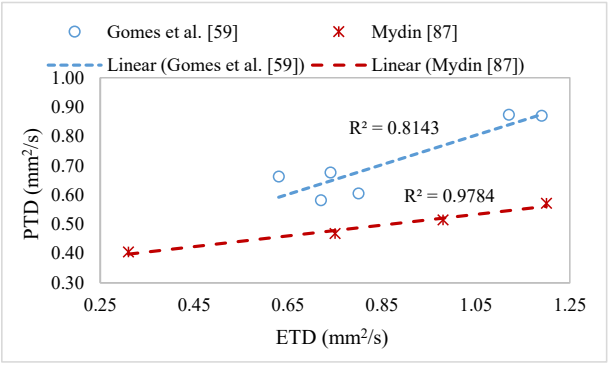

Figure 16. Validation of the proposed model (Equation 19) with previous studies.

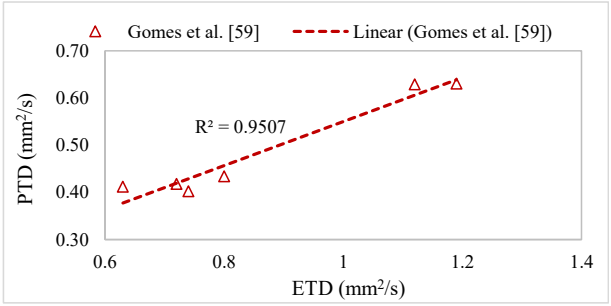

Figure 17. Validation of the developed model equation (Equation 20) with the previous study.

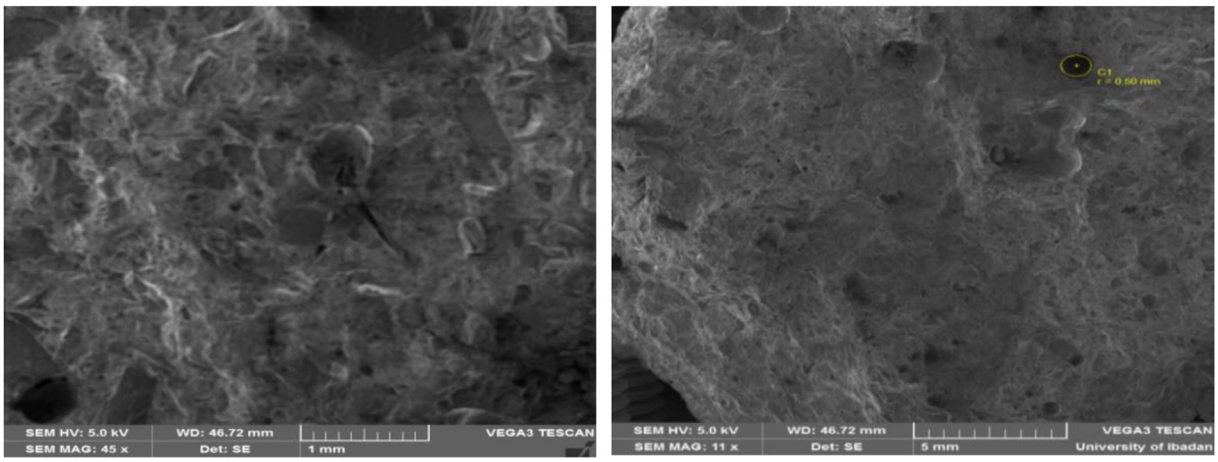

Figure 18. SEM Micrographs (a) 100% PLC concrete and (b) 95% PLC +5 % CNA concrete.

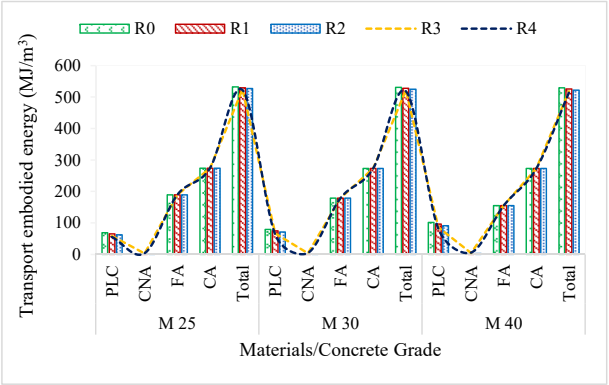

Figure 19. TEE of each construction material and concrete grade.

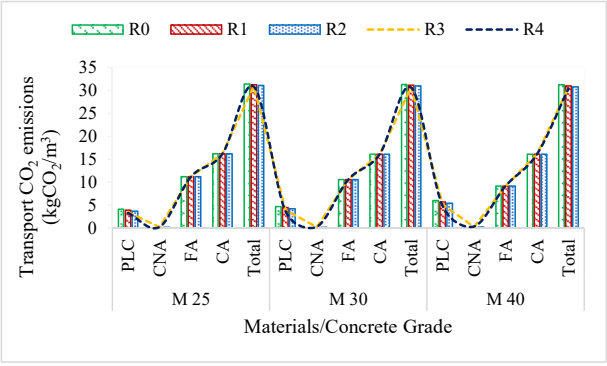

Figure 21. TEC of each construction material and concrete grade.

utilisation at 20 wt. % substitution allows a further sustainable concrete production for structural applications than conventional concrete deprived of negotiating the strength performance.

3.10.2. Embodied carbon dioxide emissions (EC)

Figure 21 shows the transport carbon dioxide emissions (TEC) of each material tonne in line with the details outlined in Tables 3, 5, and 6, and Eq. (15), using road as means of transporting each material from the production/collection source to the laboratory. The transport CO_2 emissions, particularly for CNA, in Figure 21 is vanishingly small due to its low CO_2 emission coefficient compared to other concrete components.

With references to Tables 3 and 4, and Figure 21 and Eq. (11), Figure 22 shows the EC of the concrete produced. Similar to EE, the results signified a reduction in embodied carbon dioxide emissions upon increasing the CNA content in the concrete mix. The reasons could be ascribed to the CNA's initial EC (ECi), 99 % lower than PLC. As indicated in Figure 22, the embodied carbon dioxide emissions decreased from 432.76-357.56 $kgCO_2/m^3$, 487.69–399.22 $kgCO_2/m^3$, and 608.82–498.24 $kgCO_2/m^3$ for M 25, M30, and M 40, respectively, as CNA in the concrete mix increased from 0-20 wt. %. About 5–18 % of EC were saved at 5–20 wt. % of CNA substitution for M 25, M 30, and M 40. These results support the conclusions of Abubakar et al. [39], where approximately 4–17 % of embodied carbon dioxide emissions were saved when OPC was replaced by 5–20 % of CCA in the blended cement concrete production. Li et al. [90] also found that about 4 and 19 % of embodied carbon dioxide emissions was saved at 25 and 30 % PC replacement with

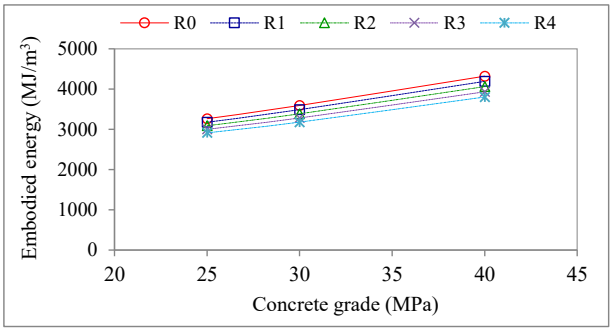

Figure 20. The embodied energy of the concrete produced.

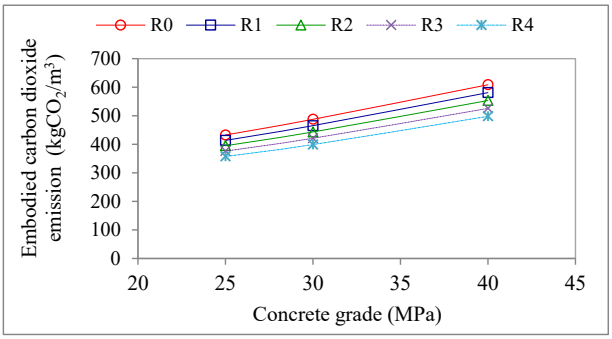

Figure 22. Embodied CO_2 emissions of the concrete produced.

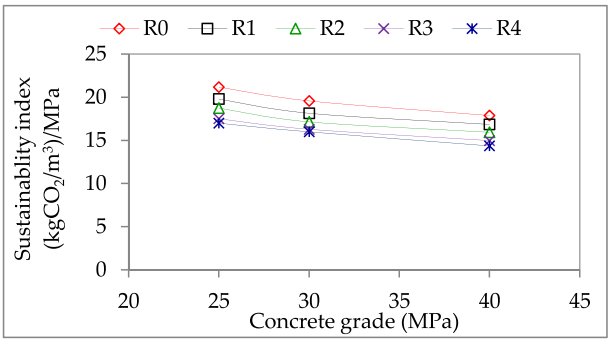

Figure 23. Sustainability index of the concrete produced at 28 days of curing.

Waste Basalt Powder (WBP). The results revealed a decrease in embodied carbon dioxide emissions upon increasing the WBP content in the concrete mix without compromising the concrete compressive strength.

Figure 22 indicates that a high cement-to-aggregate ratio also increased the embodied carbon dioxide emissions with increasing concrete grade mix. At 20 wt. % of CNA replacement, there was about 11 and 28 % increase in embodied carbon dioxide emissions as the cement-to-aggregate ratio increased by 17. 40 and 38.70 % for M 30 and M 40 compared with M 25, respectively. It is evident that incorporating CNA as a viable SCM for sustainable concrete production reduces carbon dioxide emissions and facilitates mechanical-environmental efficiency. Therefore, with 20 wt. % of CNA incorporation, the possibility exists to produce concrete with lesser embodied carbon dioxide emissions than PLC, achieving sufficient compressive strength and improving environmental performance.

3.10.3. Sustainability index (S_i)

Figure 23 presents the S_i of concrete produced. The results indicated a decrease in sustainability index as CNA in the concrete mix increased. Compared with the control concrete, R0 (100 % PLC), there was about a 7–25 % decrease in sustainability index as CNA volume in the concrete mixture augmented from 5-20 wt. % for concrete grade M 25. Similar to M 25, the sustainability index of M 30 was about 8–23 % lower than the control concrete as CNA volume in the concrete mix augmented from 5-20 wt. %. Similarly, M 40 exhibited a 6–25 % decrease in sustainability index with 5–20 wt. % of CNA in the concrete mix. These results align with Rahla et al. [91] who found an increase in concrete's sustainability by replacing PLC with SCMs (GGBFS, fly ash, and SF). Furthermore, Ashish [92] and Braganca et al. [93] pointed out that using SCMs as a partial substitute for OPC decreases the amount of cement required to make concrete, boosting its sustainability and enhancing its mechanical and durability features.

Like the EE and EC of CNA-cement-based concrete, it is pertinent to state that 20 wt. % of CNA incorporation (R4) exhibited the lowest sustainability index while also maintaining and even improving the concrete's compressive strength at 28 days of curing for all concrete grade levels, compared with the control concrete (R0). The lower the S_i, the more sustainable the concrete is [65]. Therefore, CNA is a sustainable construction material and can be used at 20 wt. % replacement with PLC without compromising the concrete's strength to produce a sustainable product for the built environment for structural and non-load bearing applications.

4. Conclusions

The present study examine the effects of CNA on the thermal and sustainability properties of cement concrete. After the experimental works and statistical analysis, the following conclusions were made:

On day 28 of curing, about a 6–23 % decrease in thermal conductivity was attained as CNA replacement increased from 5-20 wt. % for all concrete samples compared with the control concrete. The compressive strengths increased by 3–6 % as CNA replacement rose from 5-20 wt. % for all concrete samples compared with the conventional (control) concrete. Also, the SHC of the concrete increased by 2–11 % upon increasing CNA contents increases from 5-20 wt. % for all concrete grade strengths on day 28 of curing compared with the control concrete. Moreover, there was about 6–22 % decrease in thermal diffusivity as the percentage of CNA in the mix increased from 5-20 wt. % on day 28 of curing compared with the control concrete. The proposed model equations yielded high precision and strong correlation with the previous studies on day 28 of curing. In addition, there was about a 3 % decrease in concrete's embodied energy and carbon dioxide emissions at 5 wt. % of CNA content in the mix for all samples. Finally, the sustainability index reduced by about 25 % at 20 wt. % of CNA substitution for all concrete grade levels.

CNA-cement-based concrete offers better thermal insulation due to reducing density, TC, and TD. These reduce heat losses and bridge thermal effects in building envelopes, resulting in eco-friendly, sustainable, and comfortable buildings. Using CNA as a partial replacement for PLC minimises the quantity of PLC needed to produce concrete, thereby reducing the embodied energy, embodied carbon dioxide emissions, and sustainability index of concrete while maintaining and even improving the concrete's strength. These findings would help attain cleaner production and environment. However, a detailed lifecycle assessment of CNA-cement-based concrete needs to be conducted to effectively evaluate the economic benefits of using CNA in concrete production. Finally, the correlation models can be applied in designing thermal values for concrete incorporating SCMs in a building sector, reducing cost, energy, and time in laboratory work.

Declarations

Author contribution statement

Solomon Oyebisi: Conceived and designed the experiments; Performed the experiments; Analyzed and interpreted the data; Contributed reagents, materials, analysis tools or data; Wrote the paper.

Festus Olutoge: Analyzed and interpreted the data; Contributed reagents, materials, analysis tools or data.

Increase Oyaotuderekumor: Analyzed and interpreted the data; Contributed reagents, materials, analysis tools or data.

Faithfulness Bankole: Analyzed and interpreted the data; Contributed reagents, materials, analysis tools or data.

Hilary Owamah: Analyzed and interpreted the data; Contributed reagents, materials, analysis tools or data.

Ugoh Mazino: Analyzed and interpreted the data; Contributed reagents, materials, analysis tools or data.

Funding statement

This work was supported by Covenant University Centre for Research, Innovation and Discoveries.

Data availability statement

Data will be made available on request.

Declaration of interest's statement

The authors declare no conflict of interest.

Additional information

No additional information is available for this paper.

Acknowledgements

The authors would like to thank the Covenant University Centre for Innovation, Research, and Development for supporting this work financially.

References

[1] N. Atmaca, A. Atmaca, A.I. Ozçetin, The impacts of restoration and reconstruction of a heritage building on life cycle energy consumption and related carbon dioxide emissions, Energy Build. 253 (2021), 111507.
[2] M. Asim, G.M. Uddin, H. Jamshaid, A. Raza, Z.R. Tahir, U. Hussain, A.N. Satti, N. Hayat, S.M. Arafat, Comparative experimental investigation of natural fibres reinforced lightweight concrete as thermally efficient building materials, J. Build. Eng. 31 (2020), 101411.
[3] P. Zheng, H. Wu, Y. Liu, Y. Ding, L. Yang, Thermal comfort in temporary buildings: a review, Build. Environ. 221 (2022), 109262.
[4] Z. Yang, W. Zhang, M. Qin, H. Liu, Comparative study of indoor thermal environment and human thermal comfort in residential buildings among cities, towns, and rural areas in arid regions of China, Energy Build. 273 (2022), 112373.
[5] International Energy Agency, Buildings- a Source of Enormous Untapped Efficiency Potential, 2020. https://www.iea.org/topics/buildings. (Accessed 26 March 2022).
[6] T. Zhao, J. Xu, C. Zhang, P. Wang, A monitoring data-based bottom-up modeling method and its application for energy consumption prediction of campus building, J. Build. Eng. 35 (2021), 101962.
[7] A. Raihan, D.A. Muhtasim, S. Farhana, M.I. Pavel, O. Faruk, M. Rahman, A. Mahmood, Nexus between carbon emissions, economic growth, renewable energy use, urbanization, industrialization, technological innovation, and forest area towards achieving environmental sustainability in Bangladesh, Energy Clim. Change 3 (2022), 100080.
[8] A.M. Neville, Properties of Concrete, fifth ed., Pearson Education Limited, England, 2011.
[9] X. Chen, F. Zhou, D. Hu, G. Yi, W. Cao, An improved evaluation method to assess the coordination between mineral resource exploitation, economic development, and environmental protection, Ecol. Indicat. 138 (2022), 108808.
[10] W. Long, S. Wang, C. Lu, R. Xue, T. Liang, N. Jiang, R. Zhang, Quantitative assessment of energy conservation potential and environmental benefits of an iron and steel plant in China, J. Clean. Prod. 273 (2020), 123163.
[11] J. Shen, Q. Zhang, L. Xu, S. Tian, P. Wang, Future CO_2 emission trends and radical decarbonisation path of iron and steel industry in China, J. Clean. Prod. 326 (2021), 129354.
[12] R.Q. Wang, L. Jiang, Y.D. Wang, A.P. Roskilly, Energy-saving technologies and mass-thermal network optimisation for decarbonised iron and steel industry: a review, J. Clean. Prod. 274 (2020), 122997.
[13] M.Y. Liu, U.J. Alengaram, M.Z. Jumaat, K.H. Mo, Evaluation of lightweight aggregate foamed geopolymer concrete's thermal conductivity, mechanical, and transport properties, Energy Build. 72 (2014) 238–245.
[14] A. Saygılı, G. Baykal, A new method for improving the thermal insulation properties of fly ash, Energy Build. 43 (2011) 3236–3242.
[15] R. Demirboga, Thermal conductivity and compressive strength of concrete incorporation with mineral admixtures, Build. Environ. 42 (7) (2007) 2467–2471.
[16] B. Battacherjee, S. Krishnamoorthy, Permeable porosity and thermal conductivity of construction materials, J. Mater. Civ. Eng. 16 (4) (2004) 322–330.
[17] I. Budaiwi, A. Abdou, M. Al-Homoud, Variations of thermal conductivity of insulation materials under different operating temperatures: impact on envelope-induced cooling load, J. Archaeol. Eng. 8 (4) (2002) 125–132.
[18] Food and Agriculture Organization of the United Nations, Food and Agriculture Organization Statistical Pocketbook World Food and Agriculture (FAOSTAT Data), Food and Agriculture Organization of the United Nations, Rome, Italy, 2017. http://www.fao.org/3/a-i4691e.pdf. (Accessed 4 March 2022).
[19] J. Abrego, D. Plaza, F. Luno, M. Atienza-Martinez, G. Gea, Pyrolysis of cashew nutshells: characterisation of products and energy balance, Energy 158 (2018) 72–80.
[20] Cashew Handbook: Global Perspective, 2014. www.cashewinfo.com. (Accessed 4 April 2022).
[21] E.B. Mubofu, From cashew nutshell wastes to high-value chemicals, Pure Appl. Chem. 88 (1-2) (2016) 17–27.
[22] Y. Shi, P.C. Kamer, D.J. Cole-Hamilton, Synthesis of pharmaceutical drugs from cardanol derived from cashew nutshell liquid, Green Chem. 21 (2019) 1043–1053.
[23] G. Venkatakotewararao, S. Baskar, S. Arumugam, Tribological investigation of cashew nut shell oil as a lubricant additive, IOP Conf. Ser. Mater. Sci. Eng. 390 (1) (2018), 012074.
[24] T. Godjo, J.P. Tagutchou, P. Naquin, R. Gourdon, Valorization des coques d'anacarde par pyrolyse au Benin, Revue Dech. Sci.Tech. 70 (2015) 11–18.
[25] E. Aprianti, P. Shafigh, S. Bahri, J.N. Farahani, Supplementary cementitious materials origin from agricultural wastes: a review, Construct. Build. Mater. 74 (2015) 176–187.
[26] G.C. Isaia, High-performance concrete for sustainable constructions, Waste Mater. Constr. 15 (2000) 344–354.
[27] C. Pavithra, A. Arokiaprakash, A. Maheshwari, The behaviour of concrete adding chicken feather as fibre with partial replacement of cement with Cashew nutshell powder, Mater. Today Proc. 43 (2021) 1173–1178.
[28] A. Tantri, G. Nayak, M. Kamath, A. Shenoy, K.K. Shetty, Utilisation of cashew nutshell ash as a cementitious material for the development of reclaimed asphalt pavement incorporated self-compacting concrete, Construct. Build. Mater. 301 (2021), 124197.
[29] Villaquirán-Caicedo, et al., Thermal properties of novel binary geopolymers based on metakaolin and alternative silica sources, Appl. Clay Sci. 118 (2015) 276–282.
[30] G.P. Hammond, C.I. Jones, in: F. Lowrie, P. Tse (Eds.), Inventory of (Embodied) Carbon & Energy Database (ICE), University of Bath, United Kingdom, 2011. Available at: https://greenbuildingencyclopaedia.uk/wp-content/uploads/2014/07/Full-BSRIA-ICE-guide.pdf.
[31] International Energy Agency, Global CO_2 Emissions in 2019, 2020. Available at: https://www.iea.org/articles/global-CO2- emissions-in-2019. (Accessed 26 March 2022).
[32] International Energy Agency, Climate Change: the Energy Sector Is central to Efforts to Combat Climate Change, 2020. Available at, https://www.iea.org/topics/climate-change. (Accessed 26 March 2022).
[33] International Energy Agency, Cement, 2020. Available at, https://www.iea.org/reports/cement. (Accessed 26 March 2022).
[34] E. Bontempi, A new approach for evaluating the sustainability of raw materials substitution based on embodied energy and the CO_2 footprint, J. Clean. Prod. 162 (2017) 162–169.
[35] M. Hodge, J. Ochsendorf, J. Fernández, Quantifying potential profit from material recycling: a case study in brick manufacturing, J. Clean. Prod. 18 (2010) 1190–1199.
[36] K.K. Patil, C.D. Wolf, S. Chin, J. Ochsendorf, A.E. Hajiah, A. Al-Mumin, O. Büyüköztürk, Impact of embodied energy on materials/buildings with partial replacement of ordinary Portland cement (OPC) by natural pozzolanic volcanic ash, J. Clean. Prod. 177 (2018) 547–554.
[37] M.L. Berndt, Properties of sustainable concrete containing fly ash, slag, and recycled concrete aggregate, Construct. Build. Mater. 23 (2009) 2606–2613.
[38] M. González, J. Navarro, Assessment of the decrease of CO_2 emissions in the construction field through the selection of materials: a practical case study of three houses of low environmental impact, Build. Environ. 41 (2006) 902–909.
[39] A. Abubakar, A. Mohammed, D. Samson, Assessment of embodied energy and CO_2 emission of concrete containing corncob ash, Int. J. Sustain. Green Energy 10 (2) (2021) 76–84. http://www.sciencepublishinggroup.com/j/ijsge.
[40] British Standard EN 450-1: Pozzolan for Use in Concrete: Definitions, Specifications and Conformity Criteria, BSI. London, 2012.
[41] British Standard EN 8615-2: Specification for Pozzolanic Materials for Use with Portland Cement: High Reactivity Natural Calcined Pozzolana, BSI. London, 2019.
[42] American Society for Testing and Materials C 618: Standard Specification for Coal Fly Ash and Raw or Calcined Natural Pozzolan for Use in Concrete, 2012.
[43] British Standard EN 196- 3: Method of Testing Cement: Physical Test, BSI. London, 2016.
[44] British Standard EN 196-6: Methods of Testing Cement: Determination of Fineness, BSI. London, 2018.
[45] S.U. Khan, M.F. Nuruddin, T. Ayub, N. Shafiq, Effects of different mineral admixtures on the properties of fresh concrete, Sci. World J. 986567 (2014) 1–11.
[46] British Standard EN 12620: Aggregates from Natural Sources for Concrete, BSI, London, 2013.
[47] British Standard EN 206: Concrete Specifications, Performance, Production and Conformity, BSI, London, 2016.
[48] S. Oyebisi, T. Igba, D. Oniyide, Performance evaluation of cashew nutshell ash as a binder in concrete production, Case Stud. Constr. Mater. 11 (2019), e00293.
[49] S. Oyebisi, A. Ede, H. Owamah, T. Igba, O. Mark, A. Odetoyan, Optimizing the workability and strength of concrete modified with anacardium occidentale nutshell ash, Fibers 9 (2021) 41.
[50] K. Pandi, K. Ganesan, Effect of water absorption and sorptivity of concrete with partial cement replacement by cashew nut shell ash, Australian J. Basic Appl. Sci. 9 (23) (2015) 311–316.
[51] British Standard 1881-125: Methods for Mixing and Sampling Fresh Concrete in the Laboratory, BSI, London, 2013.
[52] British Standard EN 12350-2: Testing Fresh Concrete: Method for Determination of Slump, BSI, London, 2009.
[53] British Standard EN 12390- 7: Testing Hardened Concrete: Density of Hardened Concrete, BSI, London, 2019.
[54] British Standard EN 12390-3: Testing Hardened Concrete: Compressive Strength of Test Specimens, BSI, London, 2019.
[55] British standard EN 12664: thermal performance of building materials and products, in: Determination of Thermal Resistance, Using Guarded Hot Plate and Heat Flow Meter Methods, Dry and Moist Products of Medium and Low Thermal Resistance, BSI, London, 2001.
[56] C.E. Hagentoft, Introduction to Building Physics-Student Literature, 2003, p. 422.
[57] H.D. Young, R.A. Freedman, Sears and Zemansky's University Physics, tenth ed., Addison-Wesley Series in Physics, 2000, pp. 460–586.
[58] Country Club Drive, American Concrete Institute 122-14: Guide to Thermal Properties of Concrete and Masonry Systems, American Concrete Institute 38800, Farmington Hills, MI, 2014, 48331. USA.
[59] M.G. Gomes, J.A. Bogas, S. Real, B. Ferrer, A.M. Rodrigues, Experimental study on thermal properties of structural lightweight aggregate concrete, Int. J. Civ. Struct. Eng. 3 (1) (2016) 262–266.
[60] R.C. Valore, Calculation of U-values of hollow concrete masonry, ACI 2 (2) (1980) 40–63.
[61] G.P. Hammond, C.I. Jones, Embodied energy and carbon in construction materials, Proc. Inst. Civ. Eng. Energy 161 (2) (2008) 87–98.
[62] J. Yu, H.L. Wu, D.K. Mishra, G. Li, C.K.Y. Leung, Compressive strength and environmental impact of sustainable blended cement with high-dosage Limestone and Calcined Clay (LC2), J. Clean. Prod. 278 (2021), 123616.

[63] G.P. Hammond, C.I. Jones, Benchmarks for embodied energy & carbon: domestic buildings, in: Proc. Int. Conf. Soc. Sus. Environ. Eng. 07, SSEE 07), Perth: Australia, 2007.
[64] I.Z. Bribian, A.V. Capilla, A.A. Uson, Life cycle assessment of building materials: comparative analysis of the energy and environmental impact and evaluation of the ecoefficiency improvement potential, Build. Environ. 46 (2011) 1133–1140. https://doi:10.1016/j.buildenv.2010.12.002.
[65] National Energy Board, Canada's Adoption of Renewable Power Sources Energy Market Analysis, 2017, p. 27. Available at, https://www.cer-rec.gc.ca/en/data-analysis/energy-commodities/electricity/report/2017-canadian-adoption-renewable-power/2017cnddptnrnwblpwr-eng.pdf.
[66] K. Pandi, R. Anandakumar, K. Ganesan, Study on optimum utilisation of groundnut shell ash and cashew nut shell ash in concrete, Caribb. J. Sci. 53 (1) (2018) 981–991.
[67] A.A. Raheem, K.O. Oriola, M.A. Kareem, R. Abdulwahab, Investigation on thermal properties of rice husk ash-blended palm kernel shell concrete, Environ. Chall. 5 (2021), 100284.
[68] M.A. Kareem, O.O. Orogbade, E.O. Ibiwoye, N.O. Olasupo, The use of palm oil mill effluent as mixing and curing water in a cement-based composite, Silicon (2021) 1–12.
[69] K.L. Scrivener, B. Lothenbach, N. De Belie, D. Gruyaert, J. Skibsted, R. Snellings, A. Vollpracht, TC 238-SCM: hydration and microstructure of concrete with SCMs: state of the art on methods to determine the degree of reaction of SCMs, Mater. Struct. 48 (4) (2015) 835–862.
[70] V. Thirumurugan, S. George, V. Raj, K. Dheenadhayalan, Experimental study on the strength of concrete by partial replacement of cement by cashew nut shell ash (CNSA) and chicken feather fiber (CFF) as fiber reinforcement, Int. J. Adv. Res. Ideas Innov. Technol. 3 (3) (2018).
[71] British Standard EN 1992-1-1: Design of Concrete Structures: General Rules for Structural Fire Design, BSI, London, 2014.
[72] T.R. Praveenkumar, M.M. Vijayalakshmi, S. Manigandan, Thermal conductivity of novel reinforcement using TiO_2 nanoparticles and rice husk ash, Int. J. Ambient Energy 43 (1) (2022) 1127–1133.
[73] O. Damdelen, C. Georgopoulos, M. Limbachiya, Measuring the thermal mass of sustainable concrete mixes, J. Civil Eng. Architect. 8 (2014) 213–220.
[74] M.K. Howlader, M.H. Rashid, D. Mallick, T. Haque, Effects of aggregate types on thermal properties of concrete, ARPN J. Eng. Appl. Sci. 7 (2012) 900–906.
[75] J.B. Newman, in: J.L. Clarke (Ed.), Properties of Structural Lightweight Aggregate Concrete. Structural Lightweight Aggregate Concrete, Blackie Academic & Professional, Glasgow, UK, 1993.
[76] J. Newman, P. Owens, Properties of Lightweight Concrete, Advanced Concrete Technology Set, Butterworth-Heinemann, Oxford, UK, 2003.
[77] RILEM, Functional Classification of Lightweight Concretes, second ed., Recommendation LC2, 1978.
[78] M.A. Othman, Assessment of thermal conductivity, thermal diffusivity and specific heat capacity of lightweight aggregate foamed concrete, Int. J. Adv. Res. Ideas Innov. Technol. 78 (2016) 477–482.
[79] T. Ruuska, H. Kivioja Vinha, Measuring thermal conductivity and specific heat capacity values of inhomogeneous materials with a heat flow meter apparatus, J. Build. Eng. 9 (2017) 135–141.
[80] C. Ngohpok, V. Sata, T. Satiennam, P. Klungboonkrong, P. Chindaprasirt, Mechanical properties, thermal conductivity, and sound absorption of pervious concrete containing recycled concrete and bottom ash aggregates, KSCE J. Civ. Eng. 22 (2018) 1369–1376.
[81] S. Real, J.A. Bogas, M.G. Gomes, B. Ferrer, Thermal conductivity of structural lightweight aggregate concrete, Mag. Concr. Res. 68 (15) (2016) 798–808.
[82] E. Serri, A.O. Mydin, M.Z. Suleiman, Thermal properties of oil palm shell lightweight concrete with different mix designs, J. Teknol. 70 (1) (2014) 155–159.
[83] A. Kaw, W. Kalu, Adequacy of Regression Models, 2013. http://numericalmethods.eng.usf.edu.
[84] J.H. Lee, J.J. Lee, B.S. Cho, Effective prediction of thermal conductivity of concrete using neural network method, Int. J. Concr. Struct. Mater. 6 (3) (2012) 177–186.
[85] M.B. Karakoc, R. Demirboga, in: Limbachiya, Kew (Eds.), Thermo-Mechanical Properties of HSC Made with Expanded Perlite Aggregate, Excellence in Concrete Construction through Innovation, Taylor & Francis Group, London, 2009.
[86] A.A. Khan, W.D. Cook, D. Mitchell, Thermal properties of transient thermal analysis of structural members during hydration, ACI Mater. J. 95 (3) (1998) 293–303.
[87] M.A. Mydin, Assessment of thermal conductivity, thermal diffusivity, and specific heat capacity of lightweight aggregate foamed concrete, J. Teknol. Sci. Eng. 78 (5) (2016) 477–482.
[88] R. Kumar, Effects of high-volume dolomite sludge on the properties of eco-efficient lightweight concrete: microstructure, statistical modelling, multi-attribute optimization through Derringer's desirability function, and life cycle assessment, J. Clean. Prod. 307 (2021), 127107.
[89] E.R. Teixeira, R. Mateus, A.F. Camoes, L. Bragança, F.G. Branco, Comparative environmental lifecycle analysis of concretes using biomass and coal fly ashes as a partial cement replacement material, J. Clean. Prod. 112 (2016) 2221–2230.
[90] Y. Li, X. Zeng, J. Zhou, Y. Shi, H.A. Umar, G. Long, Y. Xie, Development of an eco-friendly ultra-high-performance concrete based on waste basalt powder for Sichuan-Tibet Railway, J. Clean. Prod. 312 (2021), 127775.
[91] K.M. Rahla, R. Mateus, L. Braganca, Comparative sustainability assessment of binary blended concrete using supplementary cementitious materials (SCMs) and ordinary Portland cement (OPC), J. Clean. Prod. 220 (2019) 445–459.
[92] D.K. Ashish, Concrete made with waste marble powder and supplementary cementitious material for sustainable development, J. Clean. Prod. 211 (2019) 716–729.
[93] L. Braganca, R. Mateus, H. Koukkari, Building sustainability assessment, Sustain. Times 2 (7) (2010) 2010–2023.